PCCP

Cite this: *Phys. Chem. Chem. Phys.*, 2012, **14**, 637–645

www.rsc.org/pccp

PAPER

Direct and inverse reactions of LiH^+ with $He(^1S)$ from quantum calculations: mechanisms and rates

M. Tacconi, S. Bovino and F. A. Gianturco*

Received 15th July 2011, Accepted 26th October 2011
DOI: 10.1039/c1cp22315a

The gas-phase reaction of LiH^+ ($X^2\Sigma$) with $He(^1S)$ atoms, yielding Li^+He with a small endothermicity for the rotovibrational ground state of the reagents, is analysed using the quantum reactive approach that employs the Negative Imaginary Potential (NIP) scheme discussed earlier in the literature. The dependence of low-T rates on the initial vibrational state of LiH^+ is analysed and the role of low-energy Feshbach resonances is also discussed. The inverse destruction reaction of $LiHe^+$, a markedly exothermic process, is also investigated and the rates are computed in the same range of temperatures. The possible roles of these reactions in early universe astrophysical networks, in He droplets environments or in cold traps are briefly discussed.

I. Introduction

The combination of cryogenic matrix isolation techniques and of seeded supersonic beams of atoms and molecules has led in recent years to the remarkable development of a new probing approach, *i.e.* the isolation of atomic and molecular species in ultracold (T = 0.37–0.15 K) helium droplets which are made up of 10^3 to 10^8 helium atoms.[1–4] The confined fluid environment thus formed can readily pick up atoms and molecules which can in turn form complexes with those species embedded in the interiors, or on the surface, thereby providing unique experimental opportunities.[5–8]

Such a flexible matrix has therefore been demonstrated over the years to yield a very adaptable environment, with extremely low temperatures and little matrix broadening effects, one which could also be considered for studying chemical reactions under novel conditions.[8–11]

The case for chemical reactions inside helium drops becomes even more compelling when ionic species are considered as molecular dopants inside the clusters.[8,9] In those situations, in fact, it has been shown that marked electrostriction effects are induced within the cluster,[12,13] where the ionic dopant is usually solvated well within it, and a shell-like structure of the surrounding adatoms is formed around the ionic solute, thereby allowing the selective interaction of inner-shell component adatoms with the ionic partner.[13]

Thus, we can say that to analyse the behaviour of ionic reactants with He and within He drops can indeed provide further information on low-T chemical reactions as those induced by ions in that energy range.[14]

Department of Chemistry, "Sapienza" University of Rome, P.le A. Moro 5, 00185, Rome, Italy. E-mail: fagianturco@caspur.it

There is a further, fast progressing area of chemical dynamics where low-T ionic reactions play an important role and have been accordingly pursued: the laser-cooled ionic trap environments. It has been established, in fact, that when trapped ionic species are laser-cooled to low kinetic energies, they undergo a phase transition to ordered lattice-like structures known as "Coulomb crystals", in which the characteristic inter-ion distance is typically 10–20 μm. Such structures can therefore provide an unusual source of translationally cold (~10 mK to 10 K depending on their structure) and strongly localized ions that may be trapped for long times.[14–16] Spatial imaging of such ions allows the determination of their number, thus following their disappearance in time because of some chemical process, while their Coulomb interaction could allow non-laser cooled partner species to be sympathetically cooled to similar kinetic energy values.[6,17] Such situations could therefore be thought to also provide a different environment where ionic reactions can be analyzed at low, and even ultralow energies in order to observe their general features under less conventional conditions.

In the present work we have therefore decided to analyse the computational behaviour of simple chemical partners which are expected to be amenable to the experimental detection in either helium drops or cold traps:

$$LiH^+ (X^2\Sigma^+) + He(^1S) \rightleftarrows LiHe^+ (X^1\Sigma) + H(^2S) \quad (1)$$

The above system also carries additional interest within the astrophysical community because of the role that lithium compounds, and their chemical behaviour with simple partners like H, He, and H^+, are thought to be playing in the early universe environments.[18,19] In other words, it is additionally of interest to evaluate from accurate computational sources the efficiency of reaction (1) both as a barrier-carrying reaction

leading to LiH^+ depletion, or as a barrierless reaction leading to the formation of LiH^+, with the disappearance of $LiHe^+$.

The present paper is organized as follows: the next section briefly outlines the features of our *ab initio* reactive potential energy surfaces (RPESs) for both the chemical reaction directions, while Section III summarizes our computational method for the reactive dynamics. The results for both reactive channels of eqn (1) are discussed in Section IV, while our conclusions are summarized in the final Section V.

II. The reactive potential energy surfaces: an outline

The actual numerical details of the RPESs, and of their numerical fitting procedure, have been already given in our previous work[8,20] and therefore only a few, essential features will be mentioned here in order to better understand the foregoing discussion: interested readers are referred to the above publications for additional information.

In order to guide our present discussion we report in Fig. 1 the energy profile for one of the strongest interacting paths, the one along the collinear approach.

The energy profile shown in the figure allows us to quickly assess the following:

- the reaction of LiH^+ destruction turns out to be slightly endothermic for the molecular ion in its $v = 0$ level (by above 0.05 eV), while the internally excited reagent in its $v = 1$ level takes part in an exothermic reaction leading to $LiHe^+$ formation;
- the inverse reaction for LiH^+ formation is clearly an exothermic reaction with an energy gain of about 0.06 eV from the $v = 0$ level of the $LiHe^+$ reagent.
- the complex goes through the formation of a three-particle intermediate which supports a substantial number of bound-states and exhibits a nonlinear minimum configuration for $[HeLiH]^+$.[8] The existence of this complex shall play a role in shaping the low-energy features of the reactive cross-sections in both directions, as we shall further discuss below.

The numerical fitting of the RPES has also been described before[20] and we have employed those findings to carry out reactive cross section calculations for the two branches of reaction (1), following the NIP approach discussed in the following section.

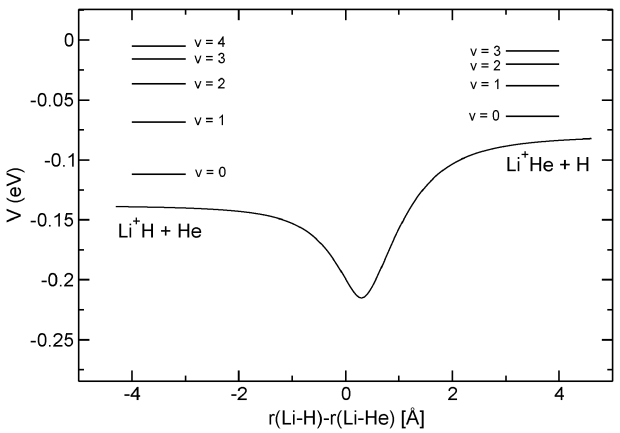

Fig. 1 Collinear profile of the RPES computed in ref. 20 for the present system. On the two sides of the reaction the energy spacings of the diatomic partners are shown: LiH^+ ($X^2\Sigma^+$) left and $LiHe^+$($X^1\Sigma^+$) right. See text for further details.

III. The quantum reactive method

The method employed in our calculations is based on the use of a Negative Imaginary Potential (NIP), as originally introduced by Baer and coworkers.[21] The leading idea is to use the NIP to convert a multiarrangement reactive system into a system where a subreactive (inelastic) problem is apparently solved while a reactive system is really being analysed.

Our approach combines the use of a NIP with a Coupled States (CS) approximation dynamics.[22] Within the CS approximation the orbital angular momentum operator $\hat{l}^2$ is assumed to be equal to $\hat{J}^2 + \hat{j}^2 - 2\hat{J}_z\hat{j}_z$ so that the couplings between different projections of the rotational angular momentum Ω along the body fixed axis are neglected thereby reducing the dimensionality of the problem. The method has proven to provide accurate reaction cross sections while reducing the computational cost,[31,35,36] especially in the case of ionic reactions.

We solve the time-independent Schrödinger equation in Jacobi coordinates at fixed values of total angular momentum, J, and its projection along the body-fixed axis, Ω:

$$\hat{H}\Psi^{J,\Omega}(R,r,\vartheta) = E\Psi^{J,\Omega}(R,r,\vartheta) \qquad (2)$$

where

$$\hat{H} = -\frac{1}{2\mu}\nabla_R^2 + \frac{\hat{J}^2 + \hat{j}^2 - 2\hat{J}_z\hat{j}_z}{2\mu R^2} - \frac{1}{2m}\nabla_r^2 + \frac{\hat{j}^2}{2mr^2} + \hat{V}(r,R,\vartheta) + \hat{V}^{\mathrm{NIP}}(r,R,\vartheta) \qquad (3)$$

The $\hat{V}^{\mathrm{NIP}}(r,R,\vartheta)$ term in the equation describes our absorbing potential. Several model forms of NIP have been proposed over the years:[21,23–27] one of the most usual forms is given by a monomial of order n:

$$\hat{V}^{\mathrm{NIP}}(r,R,\vartheta) = -iu_0\left[\frac{r - r_{\min}}{r_{\max} - r_{\min}}\right]^n \quad r_{\min} \le r \le r_{\max} \qquad (4)$$

Eqn (4) defines an isotropic absorbing potential that is acting on the whole R domain. In order to solve eqn (2) we divide the range of integration over the R coordinate into N sectors. At the mid-point ($\bar{R}_k$) of each sector we construct a local roto-vibrational adiabatic basis-set by solving the molecular Schrödinger equation:

$$\hat{h}_{\bar{R}_k}\varphi_a(r,\vartheta;\bar{R}_k) = \varepsilon_a\varphi_a(r,\vartheta;\bar{R}_k) \qquad (5)$$

where the subscript "a" is a collective index which indicates a given roto-vibrational state of the target molecule. The $\hat{h}_{\bar{R}_k}$ operator can be viewed as the molecular Hamiltonian perturbed by the presence of the colliding atom at a distance $\bar{R}_k$ from the diatom center of mass. The $\hat{h}_{\bar{R}_k}$ Hamiltonian is defined by the following equation:

$$\hat{h}_{\bar{R}_k} = -\frac{1}{2m}\nabla_r^2 + \frac{\hat{j}^2}{2mr^2} + \hat{V}(r,\vartheta;\bar{R}_k) \qquad (6)$$

The total wave function $\Psi^{J,\Omega}(R,r,\vartheta)$ is then expanded over the $\varphi_a(r,\vartheta;\bar{R}_k)$ functions:

$$\Psi_a^{J,\Omega}(r,R,\vartheta) = \sum_a G_a^{J,\Omega}(R)\varphi_a(r,\vartheta;\bar{R}_k)\,Y_J^{\Omega}(\vartheta,\phi) \qquad (7)$$

where $Y_J^{\Omega}(\vartheta,\phi)$ are the spherical harmonics and $G_a^{J,\Omega}(R)$ are the unknown translational scattering wave functions.

Substituting eqn (7) in eqn (2) we obtain the usual coupled-channel equations which are solved using an R-matrix propagator, generalized to deal with the complex algebra induced by the presence of the NIP form (as discussed in ref. 28 and 29). The R-matrix is propagated from the origin up to the asymptotic region, where the asymptotic matching conditions are enforced, thereby providing the scattering matrix (S-matrix). Because of the flux-absorbing effect of the NIP, the resulting final S-matrix is non-unitary and its default to unitarity gives us the overall reaction probability:

$$P^{J\Omega}_{(a\rightarrow \mathrm{all})} = 1 - \sum_{b} |S^{J\Omega}_{ab}|^2 \qquad (8)$$

From the reaction probability one can in turn obtain the reactive cross section in a straightforward manner by applying the formula:

$$\sigma_{(a\rightarrow \mathrm{all})}(E) = \frac{\pi}{(2j_a+1)k_a^2} \sum_{J} \sum_{\Omega} (2J+1) P^{J\Omega}_{a\rightarrow \mathrm{all}} \qquad (9)$$

IV. Results and discussion

In our approach the reactive scattering involving the forward and backward reactions sketched by eqn (1) reduces to the solution of two separate inelastic scattering problems: one in the conventionally labelled "LiH^+" arrangement (left side of eqn (1)) and the other in the "$LiHe^+$" arrangement (right side of eqn (1)). This means that two separate sets of parameters have to be tested for the two different NIPs in order to reduce the relative error of the two sets of the calculated reactive cross sections within 1%. Starting with the "LiH^+" arrangement, the length of the basis set expansion given by eqn (7) is 400 leading to an equal number of coupled equations. At each propagation sector, a converged set φ_a of molecular basis functions has been obtained by variationally solving eqn (5) and expanding φ_a over a direct product of a Colbert–Miller[30] discrete variable representation (DVR) of 150 points (ranging from $0.75a_0$ to $15.0a_0$) and a set of 43 spherical harmonics. In the case of the "LiH^+" arrangement the R-matrix has been propagated to $45.0a_0$ by using 654 sectors. Considering now the inverse reaction for the "$LiHe^+$" arrangement, the total wave function reported by eqn (5) is represented by a linear expansion of 500 elements giving an equal number of coupled equations. A converged φ_a basis has been obtained at each sector by using a direct product of a Colbert–Miller discrete variable representation (DVR) of 150 points (ranging from $0.75a_0$ to $15.0a_0$) and a set of 65 spherical harmonics. In this case the R-matrix has been propagated up to $130.0a_0$ by using 843 sectors. The calculations were carried out over a wide range of energies, from 10^{-5} to 1.0 eV, and for total angular momentum values (J) ranging from 10 to 135 for the highest energy of the forward reaction and up to 65 for the backward one. The NIP parameters were tested following the Baer criteria:[21] the NIP stability has been reached for $r_{\min} = 7.75a_0$, $r_{\max} = 11.25a_0$, and the NIP order $n = 2$ (see ref. 31 for further details) in both cases.

A. Reaction probabilities and cross sections

As mentioned in the Introduction, we have employed the NIP approach to generate first the corresponding reaction probabilities for the destruction reaction involving LiH^+

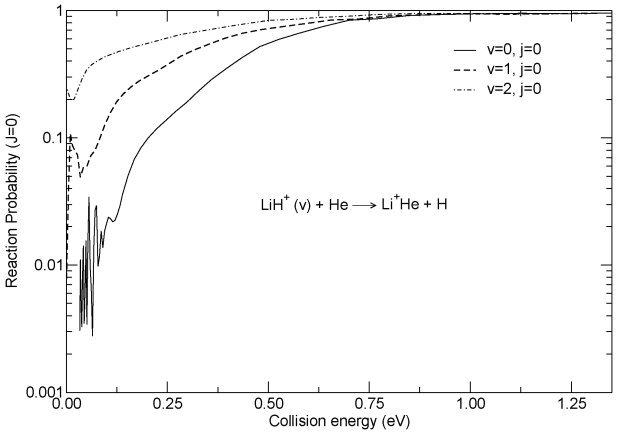

Fig. 2 Computed reactive probabilities ($J = 0$) for the LiH^+ depletion reaction at low collision energies. The curves correspond to different vibrational states of the ionic partner in the reactant region. See text for further details.

$$LiH^+ + He \rightarrow Li^+He + H \qquad (10)$$

and the data collected in Fig. 2 report these probabilities over a broad range of collision energies (given in eV) and for different values of the reagent molecule's vibrational energy content: one should notice here that the $v = 1$ and 2 initial states overcome the endothermic barrier to the products (*e.g.* see Fig. 1) and therefore the probability values can be obtained from the zero energy threshold.

Two interesting features are detected from that figure: (i) the presence of strong resonant oscillations near threshold for the $v = 0$ case, and (ii) the marked increase of the probability values at low energies as v changes from $v = 0$ to $v = 2$.

The threshold resonances in the $J = 0$ channel will be further discussed below in greater detail, while the marked increase of the reaction efficiency for vibrationally excited molecular partners might indicate the presence of an insertion reaction, *i.e.* the incoming He atom chiefly interacts with the ionic side of a stretched molecule, inserting itself between Li^+ and H, with a further out H atom as v increases. This mechanism, if present, would therefore favor a more efficient H atom detachment when the bond is further stretched and the Li^+ becomes more "isolated" from its H atom in the molecule.

In any event, this is only a qualitative suggestion that, to be further confirmed, would require additional calculations outside the main scope of the present work.

We followed a similar study for the inverse reaction that leads to the production of LiH^+, presenting the results in Fig. 3

$$LiHe^+ + H \rightarrow LiH^+ + He. \qquad (11)$$

One of the first differences for the probabilities of the inverse reaction is provided by greater values of such probabilities in the low-energy region in comparison with those given in Fig. 2.

These data indicate that exothermicity does play a significant role and that the fact that the reaction can start right up from zero collision energy implies a greater efficiency of the product formation. Furthermore, the inverse reaction still indicates a possible insertion reaction mechanism as its probabilities markedly increase with the vibrational energy content of the initial $LiHe^+$. However, this time is the H atom which

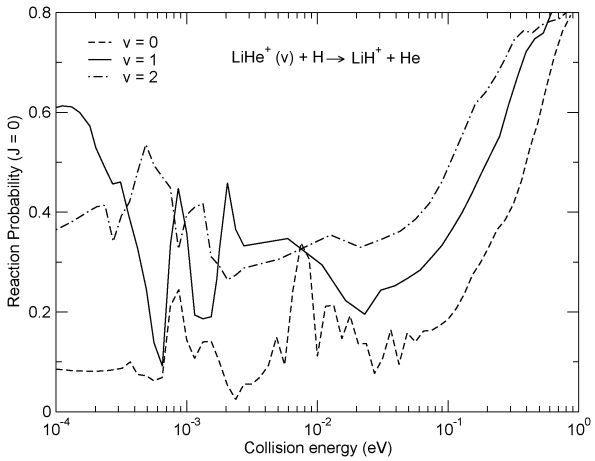

Fig. 3 Computed reaction probabilities for the inverse, exothermic reaction leading to LiH^+ formation. The different curves correspond to different vibrational states of the reagent ion $LiHe^+$. See text for further details.

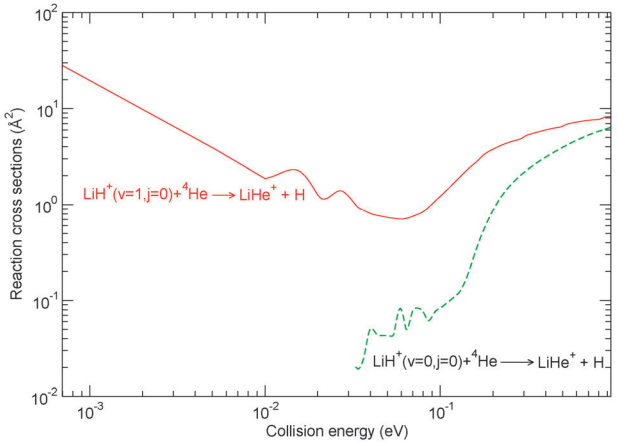

Fig. 4 Computed reaction integral cross sections for the depletion reaction of LiH^+ with He. Two different initial states of the ionic reagent are shown. See text for further details.

gets inserted into the existing bond, separating the nearly neutral He atom from the ionic partner Li^+. Additionally, we see the clear presence of resonant structures at very low energies (*i.e.* between 10^{-3} and 10^{-1} eV), all features that we shall be discussing below in more detail.

The corresponding reaction cross sections, *i.e.* the dynamical quantities which are now summed over all the contributing J values, are now given in Fig. 4 and 5.

The data in Fig. 4 show very clearly the difference between a reaction with an energy threshold (*i.e.* the process with LiH^+ in its $v = 0$ initial state) and one without, which is obviously fairly efficient at low collision energies and remains always larger than the reactions with the $v = 0$ initial state of the cation.

On the other hand, the inverse reaction that involves the formation of LiH^+ from existing $LiHe^+$ quantities, shown by the data in Fig. 5, clearly indicates how much larger these cross sections are when compared with the destruction process: between 10^{-2} and 10^{-3} eV of energies, in fact, one sees that the formation process is on average two orders of magnitude

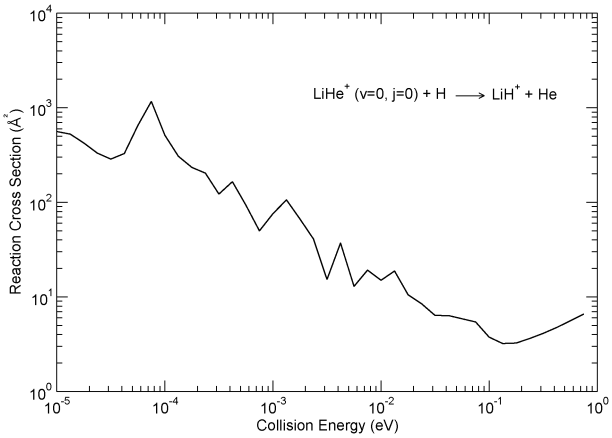

Fig. 5 Computed reaction integral cross section for the exothermic formation process of LiH^+ from $LiHe^+$ cations. See text for further details.

larger than the depletion reaction depicted in Fig. 4. In the astrophysical environment, however, one has to additionally consider the different relative abundances of LiH^+ and $LiHe^+$, based on the different concentrations of H and He atoms.

Furthermore, we see that the cross sections for the formation process of the lithium hydride cation also suggest very strong oscillating structures at low energies which do not exist for the same range and to the same extent in the case of the LiH^+ ($v = 1$) depletion process. We shall analyse such features later on, while noticing now the clear importance of complex formation during this exothermic process.

On the whole, therefore, we see that the formation reaction for LiH^+ *via* the He-route outlined here corresponds to a much more favorable process than the one involving depletion of LiH^+ ($v = 1$) *via* the same route, a feature that will be further discussed below in order to assess the survival of LiH^+ ions in the early universe models.

B. Computed reaction rates

Another important quantity that one needs to consider when modeling chemical paths involving LiH^+ and other species in

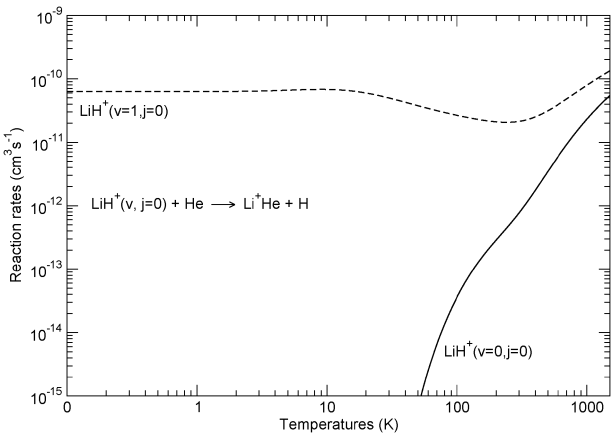

Fig. 6 Computed reaction rates for the LiH^+ depletion reactions as a function of the initial vibrational state of LiH^+ and for the considered range of temperatures. See text for further details.

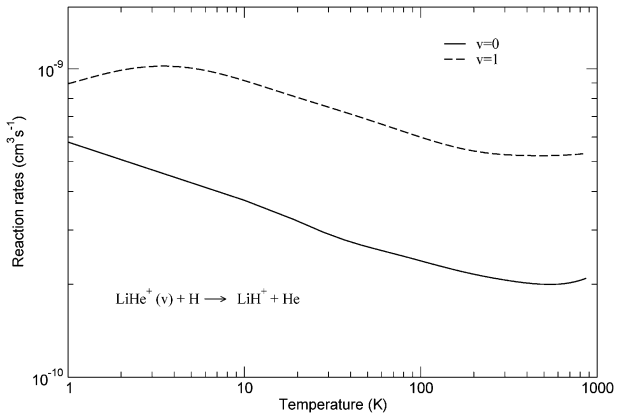

Fig. 7 Computed reaction rates, as a function of T, for the formation of LiH^+ from $LiHe^+$ in reaction with H. Two different initial vibrational states of $LiHe^+$ are considered.

the early universe environment is the behavior of the computed reaction rates from the available cross sections:

$$\alpha(T) = \left(\frac{8k_BT}{\pi\mu}\right)^{1/2} \frac{1}{(k_BT)^2} \int_0^\infty \sigma_{a\to\text{all}}(E) \exp(-E/k_BT) E \mathrm{d}E \tag{12}$$

where $\sigma_{a\to\text{all}}$ stands for the computed values of the reactive cross sections indicated in the previous subsection, $|a\rangle$ labeling the initial states of the reaction partners and "all" indicating all the final states of the reaction contributing to the flux losses in the S-matrix as obtained from the NIP approach discussed in the previous section. In the present examples only the initial vibrational state of the ionic molecular reaction may change, while no changes of the electronic state are considered in the present study: they are all out of reach for the temperatures we are considering.

The results in Fig. 6 and 7 report the calculated values of reaction rates (in units of $cm^3\ s^{-1}$) over temperature ranges between 0.1 and 1000 K.

The data reported in Fig. 6 show again the marked effect of the energy threshold: below 50 K only having LiH^+ in its $v = 1$ initial level contributes to the depletion process, which is now coming from an exothermic reaction and appears to be very efficient.

It is interesting to note, in fact, that our calculated rates for LiH^+ depletion in reaction with H[33] in the same range of temperatures as those in Fig. 6 also depend very little on T and are of the order of $10^{-9}\ cm^3\ s^{-1}$, while the present value for LiH^+ ($v = 1$) is around 7×10^{-11}, *i.e.* more than one order of magnitude slower. In other words, LiH^+ ($v = 1$) is certainly not very abundant in the early universe environments and the present study further indicates its depletion by He to be a less efficient process than that caused by the more abundant H atoms in that environments. Thus, the present reaction could be considered as only marginal for the disappearance of the initially formed LiH^+ molecular ions.

The corresponding rates for the fully exothermic inverse reaction, that of the lithium hydride cation formation, are reported by our data in Fig. 7, for two different initial states of $LiHe^+$: the same range of temperatures as in the previous case is reported in the figure. The slow dependence of this ionic reaction on T over that range of values is clear from the figure and confirms the findings for LiH^+ of before:[33] the rates vary by less than a factor of three over a T span of about three orders of magnitude.

Our data also indicate that formation of LiH^+ from this route is an interesting possibility as the rates are of about the

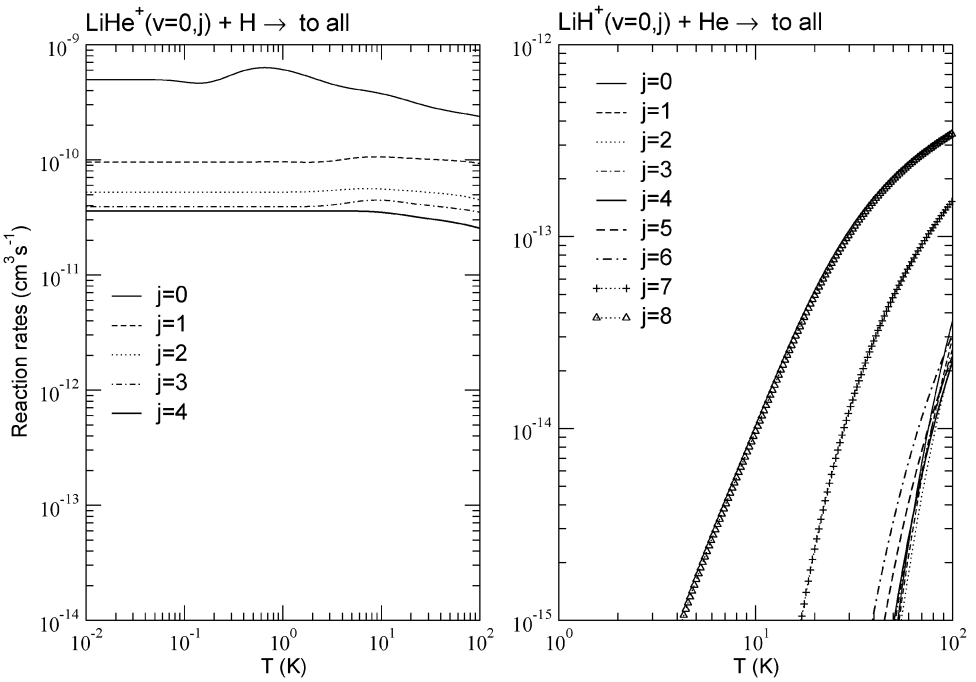

Fig. 8 Computed reaction rates at low T with molecular partners in different rotational levels but always at $\nu = 0$. Left panel: $LiHe^+$ + H reaction. Right panel: LiH^+ + He reaction. See text for further details.

same order of magnitude as those shown by the corresponding LiH^+ destruction by H (see ref. 33) and nearly two order of magnitude larger than the LiH^+ destruction by He. Thus, one may say that once $LiHe^+$ is formed in any reasonable amount, its chemical route to LiH^+ formation in reaction with H would be a barrierless, exothermic reaction with rather substantial rates that should be considered to increase the fractional abundances of LiH^+ from $LiHe^+$.[19]

C. The effect of rotational energy

In the previous subsection we have shown the effects of vibrational energy on the outcomes of the chemical reactions, both for the one with an energy threshold that presides over the formation of $LiHe^+$ (see Fig. 6) and the exothermic path for the inverse reaction that controls $LiHe^+$ destruction (see Fig. 7).

On the other hand, we know that when one studies ionic reactions in traps[15–17] it is very likely that the reacting molecules are vibrationally "cold" (*i.e.* in their ground vibrational levels) but still carry a thermal distribution within their internal rotational levels. As a preliminary test, therefore, we have further carried out calculations of low-T reaction rates where, in both directions, the molecular partners are taken to be in different rotational levels which are always $j > 0$. In the computed rates we have constrained the j_z projection to be only the $j_z = 0$ component to highlight dynamical effects but aware of the limit provided by this choice. Fuller calculations will be presented elsewhere.

The results of our preliminary calculations are shown in the two panels of Fig. 8. The right panel reports the destruction reaction for LiH^+, where we know that an energy threshold exists between reactants, as discussed in the previous sections. The various curves are associated with different rotational levels of the LiH^+ partner and clearly indicate that in the examined range of energies the partner molecules which are more rotationally excited undergo reaction more easily and, down to the few kelvins regime, the increase can span several orders of magnitude.

A qualitative, and preliminary, explanation suggests that the more internal energy is available for reaction the lower the threshold energy becomes, thereby yielding more efficient product formation of $LiHe^+$.

On the other hand, if we look at the left panel reporting the rates over the same range of temperature, but this time for the inverse reaction that causes destruction of $LiHe^+$, we clearly see that the rates become uniformly much larger than in the previous reaction, as also occurred for the rates reported earlier in Fig. 6 and 7. However, we see in this case, where no threshold exists, that putting energy into reagent molecular rotations causes the corresponding rates to become lower, albeit varying much less dramatically than those for the previous reaction.

At this preliminary stage it is difficult to say precisely which molecular mechanism may cause such changes and therefore we plan to study the effects more in detail in further studies that will appear elsewhere. However, we can already say that for both reactions, with molecular partners in their $\nu = 0$ levels, their internal rotational energy contents play a significant role in changing the size of the reaction rates, especially so when the $LiHe^+$ formation reaction is considered. Thus, the data in Fig. 8 already allow us to see that controlling the rotational energy content of ionic partners in traps is very likely to have sizeable consequences on the outcomes of the chemical reactions being considered.

D. Reaction features at ultralow energies

Because of the current general interest in ionic reactive processes at low and ultralow energies, as discussed and documented in our Introduction, we thought it to be useful to carry out a further analysis of the features of the pure reaction probabilities for the $J = 0$ component, which is the dominant one at energies from and below the meV range, in order to connect our findings with the specific properties of the RPES in the strongest interaction region between reacting partners. The analysis of these reaction probabilities is generally justified by the fact that

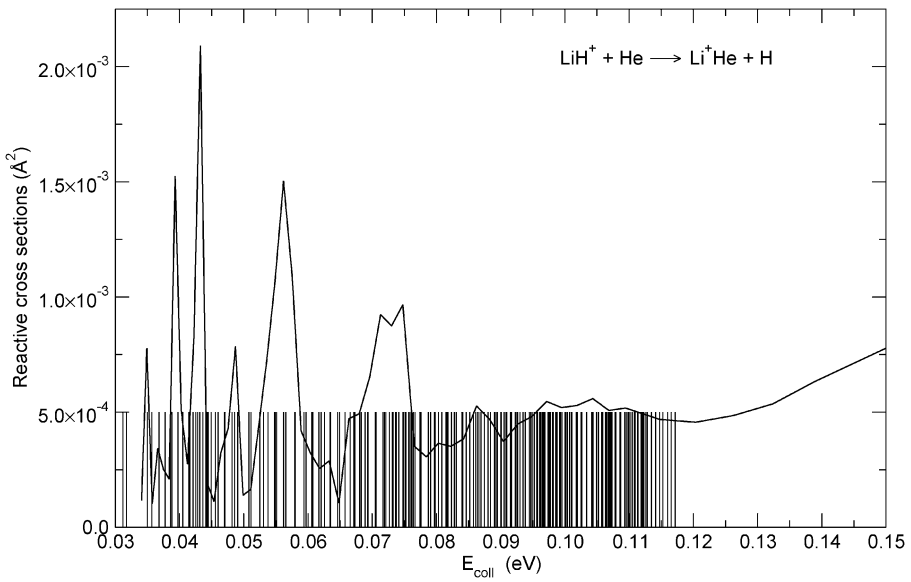

Fig. 9 Computed reactive cross sections ($J = 0$) for the formation reaction of $LiHe^+$ at low collision energies. The sequence of vertical lines reports the positions of the bound states for the adiabatic potentials of Fig. 11. See main text for further details.

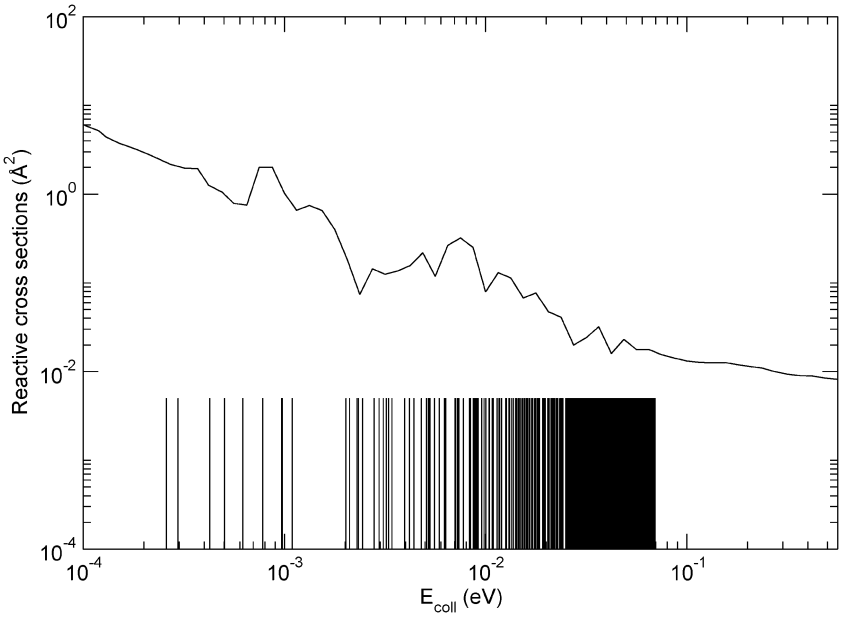

Fig. 10 Same calculations as in Fig. 9, but this time for the inverse, destruction reaction for $LiHe^+$. The vertical lines have the same meaning as those of Fig. 9 and refer to the bound states of the adiabatic potentials of Fig. 12. See main text for further details.

the "s-wave dominance" is an established property of ultracold collisional regimes.[34]

We have already seen from Fig. 3 that the reaction probabilities for the Li^+He formation channel, *i.e.* the one exhibiting an energy threshold of about 50 meV, showed strong oscillatory structures in the region from about 50 to about 100 meV, with marked intensity peaks appearing at specific energy locations. Such structures are shown more in detail by the data reported in Fig. 9, where we see the energy range for which those marked peaks are present.

Additionally, the destruction reaction for the same molecule, the one already analysed in the previous subsections, also showed marked oscillatory behaviour of its $J = 0$ reactive cross sections. Such features are reported more in detail in Fig. 10

To better understand the molecular-level mechanisms presiding over those structural features, it is important to realize first that, as shown in Fig. 1, both reacting partners' arrangements for the two reactions in Fig. 9 and 10 go *via* a complex formation stage where the local interaction added to that of the asymptotic molecules is quite important. Such additional interactions, viewed as generating a set of adiabatic potentials as discussed in Section II for each reactive arrangement, *i.e.* both for $[LiH^+\cdots He]$ and $[LiHe^+\cdots H]$, can be involved in the

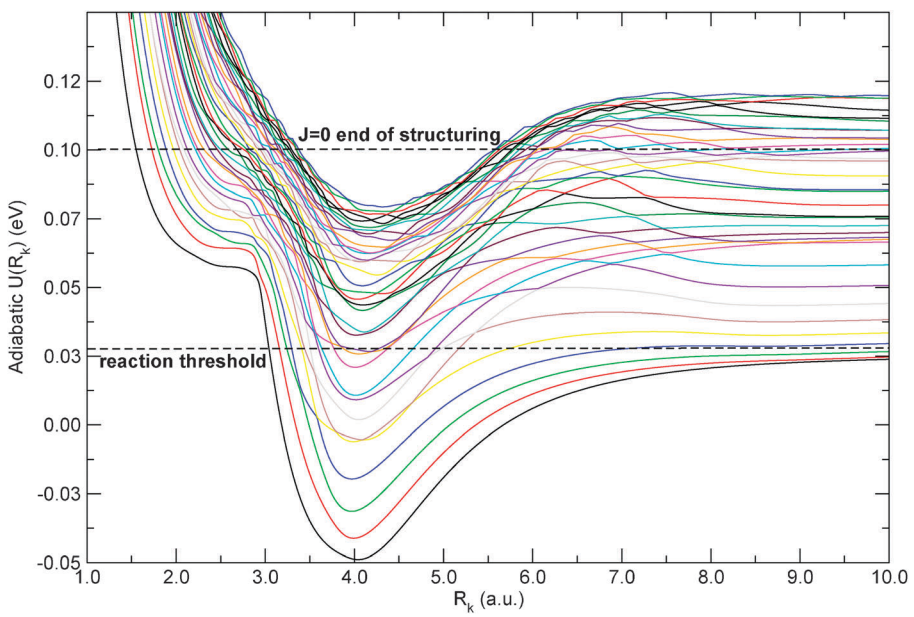

Fig. 11 Computed adiabatic potential curves, as defined in Section II, for the $LiH^+ + He$ reaction. The two dotted lines indicate the range of energy covered by the reactive cross section structures in Fig. 9.

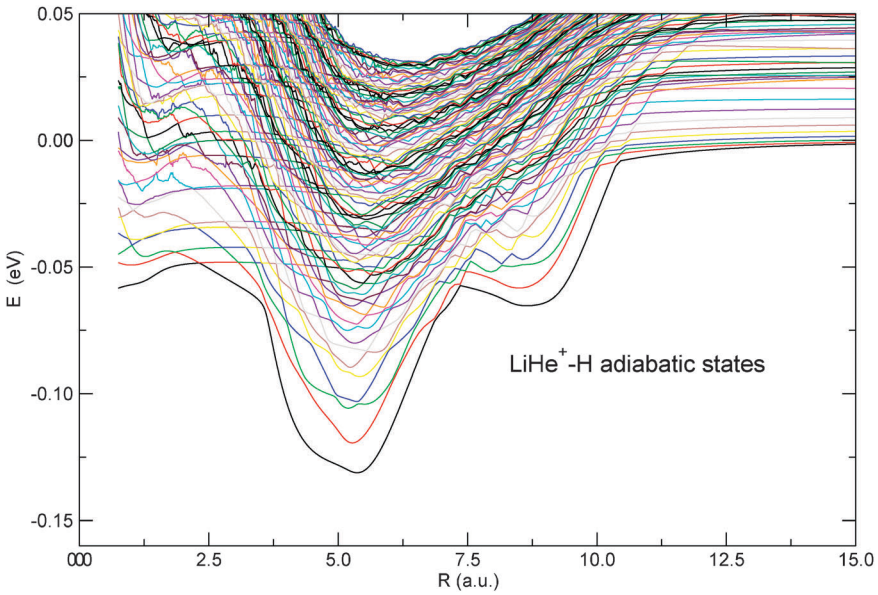

Fig. 12 Same as in Fig. 11 but for the destruction reaction of $LiHe^+ + H$. See text for further details.

occurrence of Feshbach resonances at low collision energies, where it is more likely that the attractive energy of the interactions at short ranges will cause the scattering complex to become locally bound as the system moves through the different adiabatic (vibrationally adiabatic) potentials for $LiH^+ \cdots He$ in the formation reaction and for $LiHe^+ \cdots H$ for the destruction reaction.

The data in Fig. 11 show pictorially the large set of such adiabatic potentials involving the vibrational states of the LiH^+ partner and averaged over scattering orientations.

One clearly sees there that over the shown collision energies the potentials which are asymptotically accessible become bound at short range, thereby causing the occurrence of probability-enhancing Feshbach resonances in the product channels. Due to the large number of such states supported by the potentials given in Fig. 11, we only indicate in Fig. 9 their energy location without attempting any nanoscopic classification: it is clear from the data that several hundreds of such bound states exist and several of them can cause reaction probability enhancements at specific collision energies. As that energy increases, however, the system moves too far above the well depths and therefore the coupling necessary to generate such features decreases, causing the enhancement effects to disappear.

A similar analysis is carried out for the destruction reaction structures in Fig. 10 and the corresponding adiabatic potentials are given in Fig. 12. The different vibrational structure of $LiHe^+$ is now causing a much larger number of adiabatic potentials to exist and therefore the corresponding structures in the reactive cross sections can extend over a larger range of energies. Their positions are given in Fig. 10 and one indeed sees that they now cover a much larger energy range, causing much larger enhancements in the corresponding cross sections. One could therefore say that both complex-forming ionic reactions indicate the occurrence of several Feshbach-type resonances at vanishing collision energies for the $J = 0$ case, some of which could also survive as structures when final cross sections are obtained (see Fig. 4 and 5) thereby becoming amenable to possible observation in trap studies.[14] Only when confirmed by observation one might embark into a more detailed classifications of such wealth of Feshbach resonances.

V. Conclusions

In the present work we have carried out a series of quantum reactive studies for apparently simple ionic reactions: the one involving LiH^+ destruction by He partners and the one forming LiH^+ from the destruction of $LiHe^+$ by H atoms. Both reactions have direct bearing on the construction of kinetics models for the chemical network in the early universe environment (low redshift values)[18,19] since they involve atoms with high fractional abundances (H and He) with one of the ionic molecular candidates which would be next in abundance: LiH^+.[32]

Furthermore, the reactivity of a light cation with He could be in principle tested in two other experimental environments: that involving pickup of the LiH^+ by an He droplet[10,11] and the one where a "Coulomb crystal" set-up for the cation is made to interact with a buffer gas of laser or sympathetically cooled rare gas partners.[14–17]

The present calculations have dealt chiefly with the low-T behavior of the present set of reactions and, by employing an *ab initio* generated reactive potential energy surface (RPES),[8,20] have computed the corresponding cross sections and reaction rates from a quantum treatment of the reaction dynamics that employed our in-house implemented NIP approach.[21,31,36]

The results of the present calculations indicate the following features of the reactivity in both processes:

- the LiH^+ destruction cross sections in reaction with He exhibit a marked threshold for the LiH^+ ($v = 0, j = 0$) reaction partner, thereby producing significant rates only above 100 K of temperature (see Fig. 6);
- the same reaction with a vibrationally excited partner becomes exothermic, exhibits much larger rates and indicates very efficient destruction of the molecular cation at vanishing energies;

• the LiH^+ formation reaction from $LiHe^+$, on the other hand, is a strongly exothermic reaction which starts already at zero energy and remains orders of magnitude larger than the destruction process;

• both reactions show very slow dependence on T at the temperatures of interest and therefore are expected to remain relevant for astrophysical modeling of chemical networks at low redshifts;[32]

• both reactions are shown to have rates that are enhanced by putting vibrational energy into the reacting molecules, thereby possibly suggesting a likely insertion mechanism for the partner atom with respect to the reacting cation;

• finally, both reactions are shown to exhibit marked resonances at low and ultralow energies, further indicating their possible survival as detectable structures even after the opacity summation over angular momenta. Such structures may therefore be amenable to detection in laboratory environments for low-T reactions as those outlined in our Introduction.

In conclusion, in spite of the apparent simplicity of the molecules considered, the corresponding reaction rates indicate a wealth of details which could be linked to both experiments and to improved modelings of chemical kinetics in the early universe.[19] The latter issue is currently under study in our group.

Acknowledgements

We thank both the CINECA and CASPUR Consortia for their help in making available to this project substantial computational support. The link to the COST Action on "The Molecular Cosmos" is also acknowledged.

References

1 J. P. Toennies and A. F. Vilesov, *Annu. Rev. Phys. Chem.*, 1998, **49**, 1.
2 F. Stienkemeier and A. F. Vilesov, *J. Chem. Phys.*, 2001, **115**, 10119.
3 J. P. Toennies and A. F. Vilesov, *Angew. Chem., Int. Ed.*, 2004, **43**, 2622.
4 F. Stienkemeier, W. E. Ernst, J. Higgins and G. Scoles, *J. Chem. Phys.*, 1995, **102**, 615.
5 K. Nauta and R. E. Miller, *Phys. Rev. Lett.*, 1999, **82**, 4480.
6 R. E. Miller, *Faraday Discuss.*, 2001, **118**, 1.
7 S. Grebenev, B. Sartakov, J. P. Toennies and A. F. Vilesov, *Phys. Rev. Lett.*, 2002, **89**, 225301.
8 E. Scifoni, E. Bodo and F. A. Gianturco, *J. Chem. Phys.*, 2005, **122**, 224312.
9 F. Sebastianelli, C. Di Paola, I. Baccarelli and F. A. Gianturco, *J. Chem. Phys.*, 2003, **119**, 8276.
10 M. Fárník and J. P. Toennies, *J. Chem. Phys.*, 2003, **118**, 4176.
11 M. Fárník and J. P. Toennies, *J. Chem. Phys.*, 2005, **122**, 014307.
12 M. Buchenau, J. P. Toennies and J. Northby, *J. Chem. Phys.*, 1991, **95**, 8134.
13 E. Scifoni, G. Dellepiane and F. A. Gianturco, *Eur. Phys. J. D*, 2004, **30**, 363.
14 M. T. Bell, A. D. Gingell, J. M. Oldham, T. P. Softley and S. Willitsch, *Faraday Discuss.*, 2009, **142**, 13.
15 K. Molhave and M. Drewsen, *Phys. Rev. A*, 2000, **62**, 011401(R).
16 P. F. Staanum, K. Hobybeere, R. Wester and M. Drewsen, *Phys. Rev. Lett.*, 2008, **100**, 243003.
17 A. D. Gingell, M. T. Bell, J. M. Oldham, T. P. Softley and J. N. Harvey, *J. Chem. Phys.*, 2010, **133**, 194302.
18 E. Bodo, F. A. Gianturco and R. Martinazzo, *Phys. Rep.*, 2003, **384**, 85.
19 S. Bovino, M. Tacconi, F. A. Gianturco, D. Galli and F. Palla, *Astrophys. J.*, 2011, **731**, 107.
20 M. Wernli, E. Scifoni, E. Bodo and F. A. Gianturco, *Int. J. Mass Spectrom.*, 2009, **280**, 57.
21 M. Baer, C. Y. Ng, D. Neuhauser and Y. Oreg, *J. Chem. Soc., Faraday Trans.*, 1990, **86**, 1721.
22 P. McGuire, *Chem. Phys.*, 1976, **13**, 81.
23 D. Neuhauser and M. Baer, *J. Chem. Phys.*, 1988, **90**, 4351.
24 D. Neuhauser and M. Baer, *J. Chem. Phys.*, 1989, **91**, 4651.
25 U. V. Riss and H.-D. Meyer, *J. Chem. Phys.*, 1996, **105**, 1409.
26 D. E. Manolopoulus, *J. Chem. Phys.*, 2002, **117**, 9552.
27 T. Stoecklin, *Phys. Chem. Chem. Phys.*, 2008, **10**, 5045.
28 E. B. Stechel, R. B. Walker and J. C. Light, *J. Chem. Phys.*, 1978, **69**, 3518.
29 F. Huarte-Larranaga, X. Gimenez and A. Aquilar, *J. Chem. Phys.*, 1998, **109**, 5761.
30 D. T. Colbert and W. H. Miller, *J. Chem. Phys.*, 1992, **96**, 1982.
31 M. Tacconi, S. Bovino and F. A. Gianturco, *Rend. Fis. Acc. Lincei*, 2011, **22**, 69.
32 D. Galli and F. Palla, *Astron. Astrophys.*, 1998, **335**, 403.
33 S. Bovino, M. Tacconi, F. A. Gianturco and T. Stoecklin, *Astrophys. J.*, 2010, **724**, 126.
34 E. Bodo, F. A. Gianturco, N. Balakrishnan and A. Dalgarno, *J. Phys. B: At. Mol. Phys.*, 2004, **37**, 3641.
35 S. Bovino, M. Tacconi, F. A. Gianturco and D. Galli, *Astron. Astrophys.*, 2011, **529**, A140.
36 S. Bovino, M. Tacconi and F. A. Gianturco, *Phys. Scr.*, 2011, **84**, 028103.